

Determination of the Effective Properties of Thermal Spray Coatings Using 2D and 3D Models

K. Bobzin, N. Kopp, T. Warda, and M. Öte

(Submitted April 10, 2012; in revised form June 20, 2012)

Models, which are developed to determine the effective properties of thermal spray coatings, require the material properties of each constituent of the coating as well as the information about the spatial positions and the geometries of these constituents as input parameters. The complex microstructure of thermally sprayed Yttria-stabilized zirconia (YSZ) coatings consists of irregular voids which are distributed non-uniformly in the coating. It is a common practice in the literature to employ two-dimensional (2D) cross-sectional images of the coatings to derive the geometrical model of the microstructure and conduct the simulations in 2D. In the context of this study, contrary to the 2D approach, a new three-dimensional (3D) reconstruction approach has been developed to model the microstructure of thermally sprayed coatings in 3D. The effective properties of an YSZ coating have been calculated by means of asymptotic homogenization and virtual testing methods. The results of the models, which have been conducted in 2D and 3D, are compared with each other. Finally, the capabilities of these methods with respect to the modeling approach (in 3D and in 2D) are analyzed on the basis of reference measurements.

Keywords effective coating properties, finite element method (FEM), homogenization, microstructure, simulation, thermal spraying, 3D reconstruction

1. Introduction

The mechanical and thermal properties of thermally sprayed coatings are highly dependent on the initial properties of their constituents (particles) and the morphology/microstructure of the coating. The microstructures of Yttria-stabilized zirconia (YSZ) coatings are—compared to many conventional materials—very complex. In general, they consist of inter-lamellar cracks (approximately parallel to the substrate surface) and intralamellar cracks (approximately perpendicular to the substrate surface) as well as single pores and unmelted particles (Ref 1-4).

Different methods have been implemented in the literature to characterize the microstructural characteristics of thermally sprayed coatings. Mercury intrusion porosimetry, helium pycnometry, electrochemical tests, optical image analysis, or small-angle neutron scattering are the commonest examples of these methods (Ref 4, 5). Image analysis techniques are usually based on metallographic cross-sectional images which are taken, for instance, by means of light or scanning electron microscopy. Although

the analysis of the microstructural characteristics by means of cross-sectional images is very sensitive to the correct distinction of microstructural constituents, this method is inexpensive and easy to implement, and hence, widely spread. A huge advantage of the image analysis for characterization of microstructural features is that the cross sections give detailed information about the spatial positions and dimensions of the inhomogeneities as well as their shapes and orientations. Another method to identify the characteristics of the microstructure is the x-ray microtomography (XMT). A three-dimensional (3D) view of the microstructure can be created by measuring the attenuation of x-rays along the sample in different directions. Although the XMT method—compared to the other methods—is easier and faster to carry out, it has only a limited capability to determine small pores and inhomogeneities, which are characteristic for thermally sprayed coatings (Ref 5-7).

Thermally sprayed coatings are in general considered to be non-uniform in all spatial directions. In the case of 3D heterogeneous media, such as fiber-reinforced composites, which can be considered as periodic or random along two directions and uniform along one direction, the calculation of the effective properties done by analyzing the two-dimensional (2D) structure will be equivalent to one with 3D structure. The reduction of the problem domain from 3D to 2D is a possible factor limiting the prediction capability of the numerical models, especially for the structures which do not show any uniformity in a particular direction. Although the uniformity along the third direction is a critical quality criterion for 2D approach, it is still a common practice adopted in the literature to model thermally sprayed coatings using the

K. Bobzin, N. Kopp, T. Warda, and M. Öte, Surface Engineering Institute, RWTH Aachen University, Kackertstr. 15, 52072 Aachen, Germany. Contact e-mail: oete@iot.rwth-aachen.de.

2D cross-sectional images (Ref 8-16). Since experimental methods (i.e., XMT) are not yet capable of capturing a 3D view of the microstructure with all the details (Ref 6, 7), generating 3D views of the coatings out of the 2D images is claimed as an active research area in the literature (Ref 5).

In the present study, a pragmatic approach has been developed, which makes the generation of 3D representation of the YSZ coatings become simple and straight forward. By means of numerical analyses, conducted in 2D and 3D, the effective Young's Modulus and thermal conductivity of thermally sprayed YSZ coatings have been computed. On the basis of reference measurements, the capabilities of the different methods to determine the effective properties have been analyzed.

2. Material and Processing

As a spraying material, ZrO_2/Y_2O_3 93/7 (YSZ, H.C. Starck GmbH, Goslar, Germany) with a fraction size of $-90+16\ \mu\text{m}$ has been used. Spraying parameters for the air plasma spraying (APS) system TriplexPro-210 (Sulzer Metco Europe GmbH, Kelsterbach, Germany) are listed in Table 1. As coating thickness about $350\ \mu\text{m}$ has been realized, the resulting porosity has been around 23%. Thickness and porosity of the coating have been measured by means of image analysis.

3. Numerical Methods

The material properties of the coating constituents and information about their morphology and spatial positions, which are derivable from the cross-sectional image, form the basis of the analysis for the determination of the effective coating properties. In previous studies, different methods have been implemented to determine the effective properties of the coatings. In some of these studies, analytic relationships between the microstructural features and the effective coating properties have been established by idealizing the complex microstructure of the coating with simplifications (Ref 3, 17-21). However, these simplifications limit the predictive capability and the accuracy of the analytic models. The numerical approach, which is based on the real microstructure of the coating, represents an approach with a greater promise for the determination of the effective properties. The averaging process, which performs the micro-macro transition to

determine the influence of the inhomogeneities of the microstructure on the macroscopic properties, is called homogenization. Homogenization methods are based on the assumption that a specific small part of the microstructure can be considered to be representative for the entire material. Therefore, the dimensions of the so-called representative volume element (RVE) are much smaller than those of the entire microstructure. However, the RVE must contain sufficient number of microstructural inhomogeneities, so that the morphology of the RVE is equivalent to the entire microstructure (Ref 22, 23). Two different homogenization methods have been employed in the context of this study. The first one is based on the asymptotic expansion of the involved fields and assumes the periodicity of the microstructure. For materials with periodic microstructure, this method predicts the effective properties accurately and efficiently with regard to time consumed. For non-periodic microstructures like APS thermal barrier coatings, the geometrical definition of the RVE plays a crucial role. In fact, these microstructures are approximated by periodic ones, characteristics of which are obtained by statistical methods. Hereafter, this method will be called asymptotic homogenization. The software tool HoMat[®] (Ref 24, 25), which is based on the asymptotic homogenization, has been employed to predict the effective properties of the coating. Here, the macroscopic solution is treated as the limit of microscopic solutions of the family of differential operators depending on a small, scale ratio parameter. Please refer to the study of Bobzin et al. (Ref 26) for the theory of this method. The second numerical homogenization method to determine the effective properties of thermally sprayed coatings is based on the finite element analysis (FEA). The position-dependent stress and strain behaviors of the RVE under a constant external load, which are subsequently used to calculate the effective properties, can be determined using the finite element method (FEM). In this regard, the boundary conditions of the FEA should be defined by virtual replication of a mechanical or thermal load. Therefore, in the literature, this method is referred as virtual testing method (Ref 26). The effective Young's modulus and thermal conductivity of the coating can be predicted from the calculated stresses and strains (Ref 8). In this study, the definition of the boundary conditions and the calculation of the stress-strain behavior are conducted using the commercial numerical analysis program Altair Hyperworks v11.0[®].

The discretization of the RVE with sufficiently small FEs, which allows a realistic approximation of the microstructure, is the prerequisite for the above mentioned homogenization methods. In this regard, the cross-sectional images of the coating should be converted into FE-based geometry files. For this purpose, first of all, the different constituents in the microstructure should be tagged by assigning different discrete colors to corresponding pixel sets. The open-source program OOF2, which was developed at the United States National Institute of Standards and Technology (NIST), has been often employed in the literature to convert the cross-sectional image files (Ref 27, 28).

Table 1 Spraying parameters for the APS system TriplexPro-210

1. Gas (Argon)	60 SLPM
2. Gas (Nitrogen)	8 SLPM
Current	450 A
Stand-off distance	170 mm
Nozzle	9 mm

3.1 2D Models

The Zeiss Axiophot Fluorescence microscope has been implemented to capture the $\times 200$ magnified cross-sectional images of the coatings (2580×1944 pixels). Visual rendering of the images has been improved using the Retinex algorithm of the GNU Image Manipulation Program[®] (GIMP) to enhance the contrast and overcome the problems because of the non-uniform lighting conditions. By selecting regions with similar colors and assigning them black and white colors, the cross-sectional light microscopy images of the coating have been converted into two-color images. The voids (pores and cracks) are tagged with black, and YSZ is tagged with white color. The two-color images of randomly extracted windows have been converted into FE-based geometry files using the open-source object-oriented FE program OOF2. The generated geometry files have been imported into Hyperworks[®] for further processing. The error introduced because of the plane stress or plane strain assumption has been eliminated by extruding the geometry in the third direction (see Fig. 1)

3.2 3D Models

Since the assumption “uniformity of the third direction” does not hold for thermally sprayed coatings, the 2D models have a restricted ability to simulate the true behavior of the coatings. Wiederkehr et al. reconstructed the 3D view of coatings by mutually aligning 2D images, which were cut out of the cross-sectional images of the coating lying parallel to each other. The parallel cross-sectional images were acquired by successively grinding and polishing the specimen (Ref 5). The microstructure of a medium, which consists of random inhomogeneities, is unique. The windows, which are cut out from different locations of this microstructure, represent uniqueness as

well. Stating this, homogenization with RVEs from different spatial positions will theoretically deliver different effective properties for the same coating. In order to find out a global property, which is valid for the whole structure, the definition of the RVE should ensure that the deviation between the effective properties calculated using different RVEs is insignificantly small. For this purpose, instead of defining the 3D RVE at a predefined location, several 2D images, which are selected randomly from different locations on the same cross-sectional image, have been used in this study to reconstruct a 3D-representation of the coating. First of all, the randomly selected 2D images have been converted into FE-based geometries and aligned in random order along the third direction. By extruding the FEs along the third direction and tying them together (one-to-one connection), the 3D representation of the RVE has been derived (Fig. 2). With the help of this statistical 3D reconstruction approach, the randomness of the microstructure has been taken into consideration for the definition of the RVE while eliminating the extensive grinding and polishing steps.

The variation in dimensions of single voids in z -direction cannot be captured using the 3D reconstruction approach. Nevertheless, the spacing between the 2D images of the 3D representation corresponds to the average void dimension in z -direction. Based on the common consideration that the thermal spray coatings show similar characteristics in directions parallel to the deposition surface (x - and z -directions), the average dimensions of the voids laying in xy -plane should confirm with the average dimension of the voids laying in yz -plane. Therefore, an appropriate averaging method, which is conducted over the void dimensions in xy -plane, can be implemented to determine the spacing between the levels of 3D representation in z direction. In the case of a

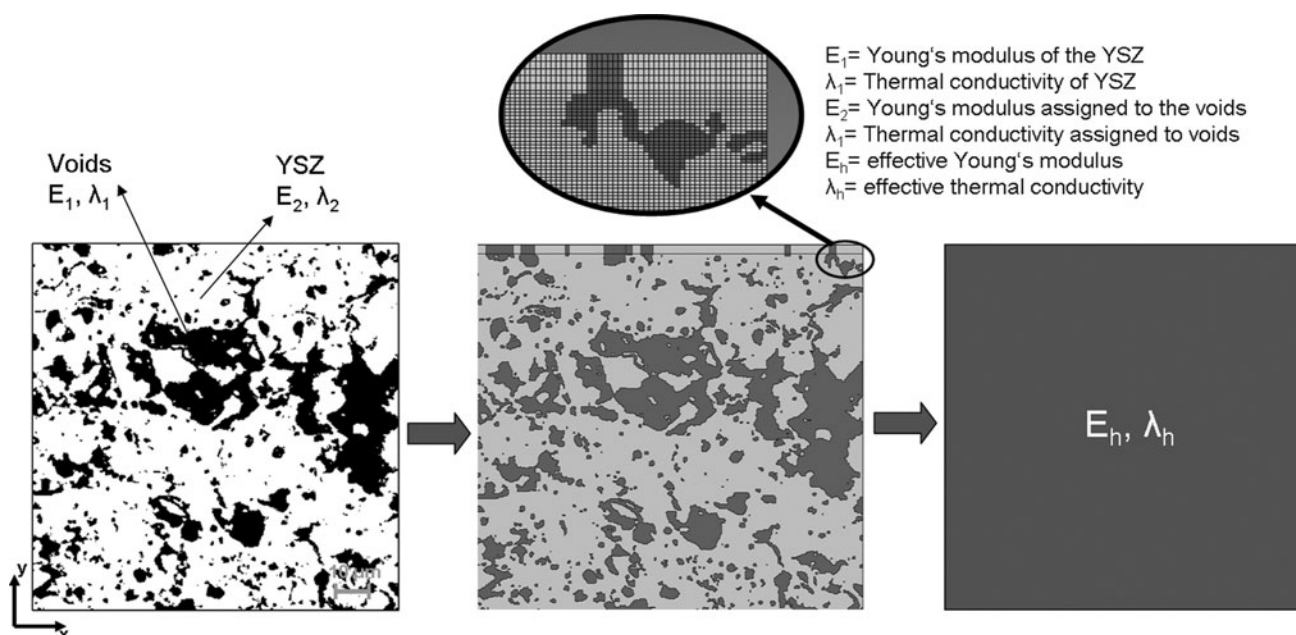


Fig. 1 Homogenization of thermal spray YSZ coatings obtained by 2D approach

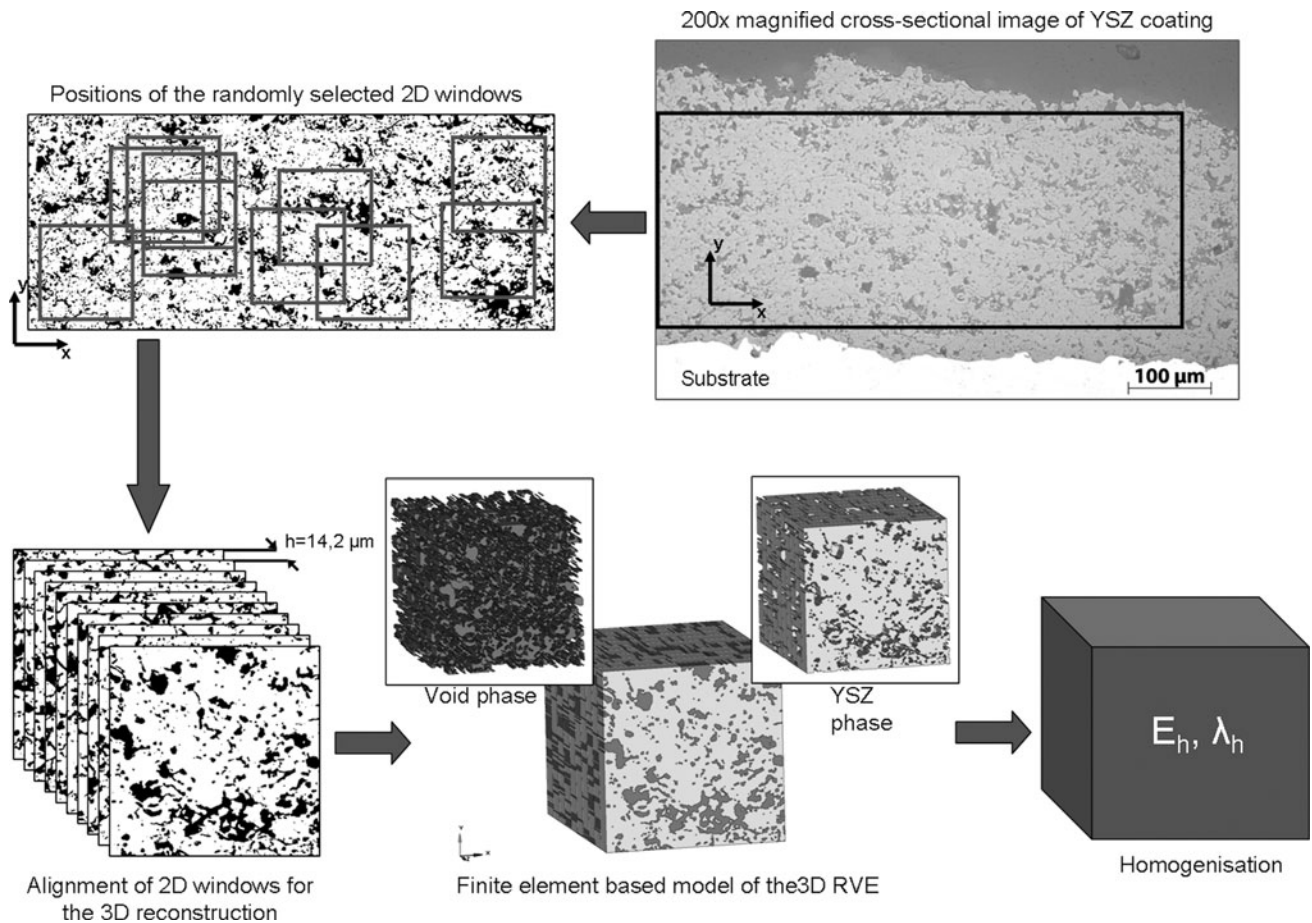


Fig. 2 Homogenization of thermally sprayed YSZ coatings obtained by statistical 3D reconstruction approach

coating microstructure which consists of inhomogeneities with very high aspect ratios (cracks), i.e., microstructure of a cold spray coating, the averaging is conducted over the length of individual inhomogeneities. In this study, in which the voids with small aspect ratios are dominant, the spacing between each pair of 2D images (h) has been calculated by averaging the idealized diameters of individual voids in xy -plane. First of all, the surface areas of each single void (F_i) in the microstructure have been calculated from the dimensions of the corresponding pixels. The idealized diameter of each void (θ_i) has been determined using the following relationship:

$$\theta_i = \sqrt{\pi F_i}$$

The weighted average of the idealized void diameters ($h = 14.2 \mu\text{m}$), which is calculated using the following relationship, has been deployed as the length of the spacing between the 2D images, where n is the total number of the individual voids.

$$h = \frac{\sum_i^n F_i \theta_i}{n}$$

Depending on the discretization level, linear FEs can cause an artificial stiffness because of their limited degrees of freedom for various types of deformation. Analyses that

have been conducted using higher discretization levels have proved that the 3D models which are reconstructed using a single layer of linear FEs between 2D windows show over-stiff behavior. In the case of models with five layers of linear FEs, results of the discretized problem converge to a solution which changes only insignificantly as the number of layers increased further. Since the solution of the models with one single layer of higher-order (quadratic) elements does not differ from the solution of the model with five layers of linear FEs significantly ($< \sim 5\%$) and leads to considerable savings in computation time and resources, the virtual testing models have been reconstructed using single layer of higher-order (quadratic) FEs. For the asymptotic homogenization method, on the other hand, five linear FE layers had to be defined between each pair of 2D windows, because HoMat[®] does not support higher-order FEs. Linear elastic material model has been employed to define the material properties of the constituents of the coating. Although the void phase in the microstructure is considered not to have any stiffness, it has been still modeled as elastic medium with a Young's modulus of $E_2 = 100 \text{ MPa}$, which is much smaller than the Young's modulus of YSZ ($E_1 = 210000 \text{ MPa}$). The aim was to prevent the possible numerical instability and erroneous microscopic displacements. A

thermal conductivity value of $\lambda_2 = 0.025$ W/m K, which is comparable with the conductivity of air at room temperature, has been assigned to the void phase. A thermal conductivity value of 2 W/m K has been assigned to the YSZ phase. For the virtual testing, the boundary conditions have been defined as illustrated in Fig. 3.

As seen in Fig. 3, stiff shell elements have been employed on the sides of the 3D model to prevent erroneous microscopic displacements due to excessive nodal loading. The influence of unphysical lateral contraction of the elements neighboring to the stiff shell elements on the results have been minimized by defining the magnitude of loading so small that the overall stresses on the elements do not lead to a significant necking-like deformation on these elements. Assuming that the accumulated strain energy in the inhomogeneous medium is equivalent to the strain energy accumulated in homogenous medium (Ref 29), the effective Young's modulus (E_h) of the microstructure can be determined from the computed element stresses and strains using the following equation:

$$E_h = \frac{(F^2/A^2)V}{\sum \sigma_{ij}\epsilon_{ij}},$$

where F is the total force applied, A is the cross-sectional area of the calculation domain perpendicular to the loading direction, V is the volume of the calculation domain, σ and ϵ are sequentially the calculated stresses and strains of the FEs, and the indices i and j represent the spatial directions. Similarly, based on the assumption that the heat fluxes in inhomogeneous and homogenous medium are equivalent in the loading direction (Ref 29), the effective thermal conductivity (λ_h) of the coating can be calculated using the following equation:

$$\lambda_h = \frac{d}{(T_1 - T_0)} \frac{\sum_i^n \Delta T_{i,j} \lambda_i}{n},$$

where d is the thickness of the calculation domain in the loading direction; T_0 and T_1 are the temperatures at the

opposite edges of the window; ΔT_i and λ_i are, respectively, the temperature gradient and thermal conductivity of the i th element in the calculation domain; the index j represents the spatial direction of the loading; and n is the total number of the elements.

4. Experimental Methods

The effective elastic properties of thermally sprayed coatings can be determined by means of different experimental methods, such as the uniaxial tensile test, 4-point bending test, micro-/nanoindentation, and ultrasound test. In the tensile test/4-point bending test, the relationship between the elastic deformation of the specimen and the Young's modulus/flexural modulus is determined according to the force and the moment equation. The ultrasound test is a non-destructive method in which the resulting acoustic emissions of the oscillations caused by a mechanical pulse are recorded. The physical relationship between the velocity of the ultrasonic wave in the material and the material properties allows the determination of the Young's modulus of the specimen. In indentation methods, a Vickers or Berkovich diamond is pressed into the surface of the sample. The continuous recording of the active force and the resulting penetration depth allows for the determination of the indentation hardness and indentation modulus. The indentation modulus (E_{IT}) is comparable to the modulus of elasticity but not identical with it (Ref 30). Microindentation was frequently used in the literature to measure the effective Young's modulus of coatings and to verify the simulation results, because the method is versatile, practical, and easy to implement. In general, the laser flash method is deployed in the literature to determine the thermal conductivity of thermally sprayed coatings. In this method, the upper side of the sample is heated with the laser, and simultaneously, the temperature on the rear side of the sample is recorded

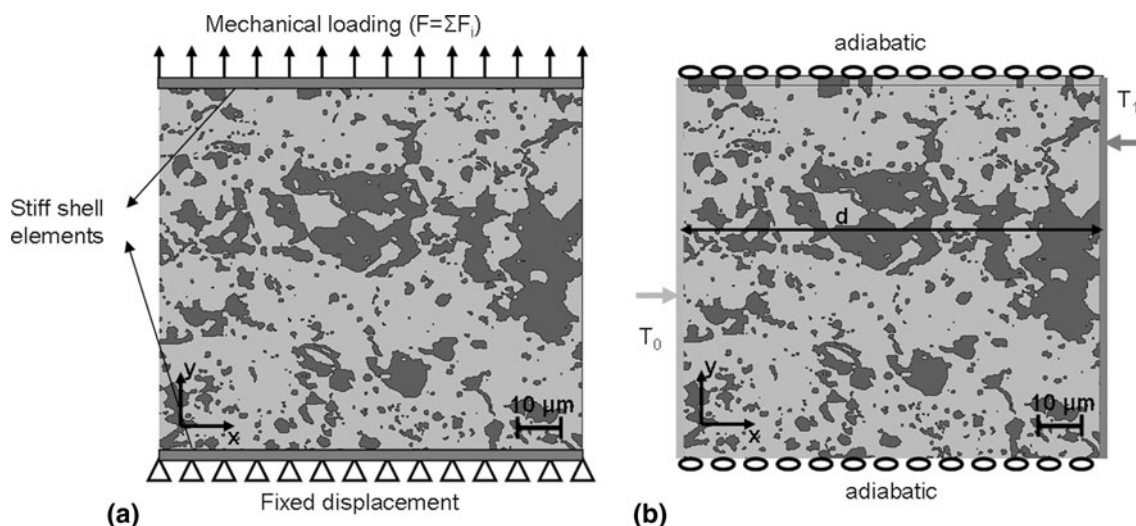


Fig. 3 (a) Mechanical boundary conditions, loading in y direction; and (b) thermal boundary conditions, loading in x direction

using an infrared detector. From the relationship between heat capacity, density, and temperature conductivity, the actual thermal conductivity of the sample can be determined (Ref 31). In this study, microindentation and laser flash method have been employed to determine the mechanical and thermal properties of the coatings. Forty-three microindentation measurements have been conducted on the cross section of the coating according to the European standard EN ISO 14577 (Ref 30) using the instrument Fischescop[®] HM2000 XYp. The thermal conductivity measurements have been carried out using the instrument LFA 447 NanoFlash[®] over three different samples. Each sample has been characterized six times. Since the measurements of temperature conductivity in the in-plane directions are challenging, the measurements have been executed only in direction perpendicular to deposition surface.

5. Results and Discussion

For heterogeneous materials with periodical microstructure, the RVE is defined by the unit cell of the periodic microstructure, and the choice of the position of the RVE is not important. In contrast to periodic microstructures, it is a sensitive and a non-trivial task for materials with random inhomogeneities, i.e., thermally sprayed coatings, to define the size/morphology of the RVE. In this study, the standard deviations of the Young's moduli, which have been calculated using different 3D models reconstructed from several random 2D images, have been analyzed to define RVE. Through systematic replacement of the smaller models with larger ones, the change in the standard deviation (σ) has been investigated. The calculations have been conducted using the asymptotic homogenization method. Since the large-scale models involve higher number of inhomogeneities, which ultimately influence the effective properties of the coating, the standard deviation of the results decreases as the size of the model increases. The Young's moduli and the thermal conductivities in the x -direction (E_x , λ_x) and in the y -direction (E_y , λ_y) have been computed with four different 3D models which have been reconstructed using four different sets of 20 random 2D images with dimensions of $54 \times 54 \mu\text{m}^2$ (see Table 2).

The sufficiently small value of the standard deviation (less than $\sim 7\%$ of mean E_x/E_y and less than $\sim 3.5\%$ of mean λ_x/λ_y) ensures that the effective properties calculated with a RVE with these dimensions do not significantly depend on the local positions of the 2D images, which have been used to reconstruct the 3D model. In other words, it shows that the dimensions of the RVE are large enough to be significantly representative for the whole structure. Nevertheless, owing to the available computational capacity, a larger model has been employed for further evaluations to assure a better representation of the microstructure and to increase predictive capability of the model. Ten randomly selected 2D windows with dimensions of $108 \times 108 \mu\text{m}^2$ have been implemented to reconstruct this 3D model. As an example, the element results of this model, which are calculated using FEM in the context of virtual testing method, are represented in Fig. 4.

The mean indentation modulus of the coating, which is gathered through microindentation measurements on 43 different points over the whole cross section of the coating matches with the effective properties calculated with homogenization methods very well (see Table 3). As a consequence of the reduction of stiffness in the perpendicular direction due to inter-lamellar cracks and weak splat boundaries, the Young's modulus of thermal sprayed coatings in the in-plane direction (E_x) is in general higher than the one in the perpendicular direction (E_y) (Ref 32). Similarly, the differences in the calculated λ_x and λ_y can be explained with the characteristic lamellar structure of the coatings.

For further evaluation, the mean value of the results of ten different 2D simulations, which have been calculated using the 2D images involved in the reconstruction of the 3D representation, is determined. Relatively high values of standard deviation have been reached even with a relatively large window size ($108 \times 108 \mu\text{m}^2$) (Table 4). This shows the higher sensitivity of the results calculated with 2D RVEs to the spatial position, in contrast to those with 3D RVEs. Homogenization of 2D windows with dimensions larger than $108 \times 108 \mu\text{m}^2$ did not result in further significant reduction in the standard deviation. Therefore, the mean value of the effective properties calculated using 2D RVEs with these dimensions has been used for the evaluations. The results calculated by virtual testing method are clearly lower than the ones calculated by asymptotic

Table 2 Calculated effective properties (E = Young's modulus, λ = thermal conductivity) of the four different 3D samples obtained using statistical 3D reconstruction approach

Sample	Method	h , μm	Dimensions, μm	E_x , GPa	E_y , GPa	λ_x , W/m K	λ_y , W/m K
Set 1	3D asymp. hom.	14.2	$54 \times 54 \times 71$	105.5	91.3	1.24	1.15
Set 2	3D asymp. hom.	14.2	$54 \times 54 \times 71$	103.2	95.0	1.23	1.18
Set 3	3D asymp. hom.	14.2	$54 \times 54 \times 71$	90.4	84.9	1.15	1.11
Set 4	3D asymp. hom.	14.2	$54 \times 54 \times 71$	97.7	86.9	1.18	1.11
Mean value μ (Set1-Set4)				99.2	89.5	1.20	1.14
Standard deviation σ (Set1-Set4)				6.7	4.5	0.04	0.03

h : distance between each pair of 2D images

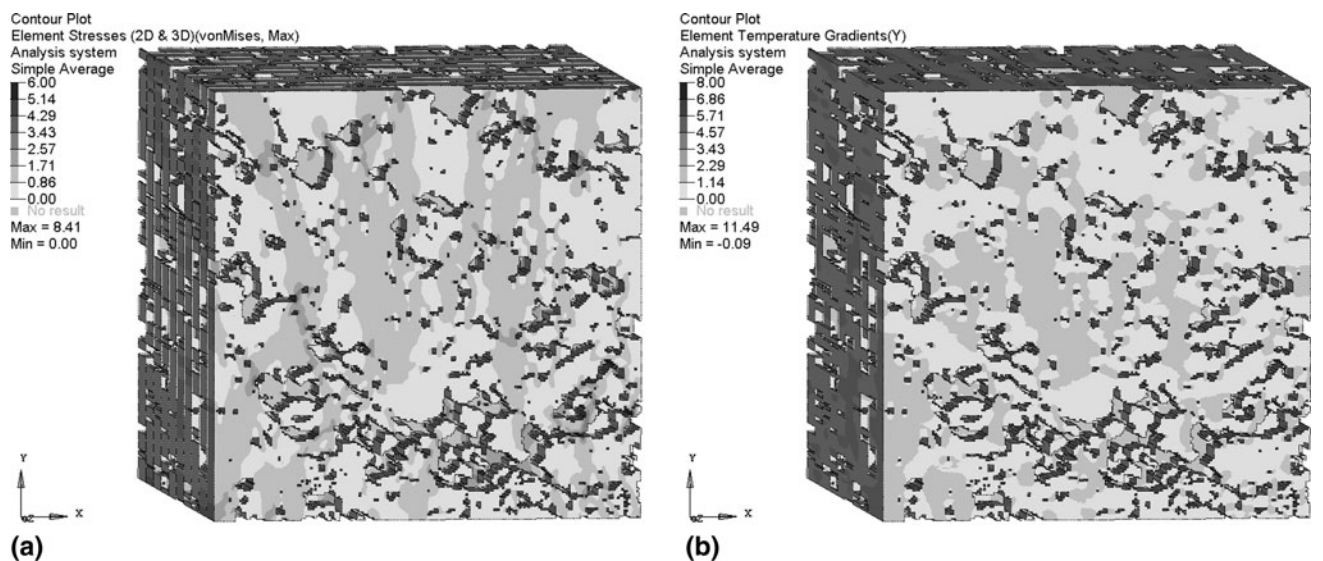


Fig. 4 (a) Element stresses (Mpa) under mechanical loading in y direction, and (b) element temperature gradients (K) under thermal loading in y direction

Table 3 Effective properties calculated using the 3D approach as well as the measured properties

Method	h , μm	Dimensions, μm	$E_{x/TT}$, GPa	E_y , GPa	λ_x , W/m K	λ_y , W/m K
3D virt. test.	14.2	$108 \times 108 \times 142$	97.6	82.3	1.24	1.17
3D asymp. hom.	14.2	$108 \times 108 \times 142$	99.0	87.1	1.19	1.11
Microindentation	n/o	n/o	$\mu = 96.0$ $\sigma = 11.0$	n/o	n/o	n/o
Laser flash (at room temperature)	n/o	n/o	n/o	n/o	n/o	$\mu = 1.07$ $\sigma = 0.05$

Table 4 Effective properties calculated using the 2D approach

Method	Dimensions, μm	E_x , GPa	E_y , GPa	λ_x , W/m K	λ_y , W/m K
2D virtual testing	108×108	$\mu = 66.2$ $\sigma = 16.5$	$\mu = 40.0$ $\sigma = 16.0$	$\mu = 1.03$ $\sigma = 0.14$	$\mu = 0.86$ $\sigma = 0.16$
2D asymp. hom.	108×108	$\mu = 77.0$ $\sigma = 15.1$	$\mu = 55.9$ $\sigma = 15.5$	$\mu = 1.07$ $\sigma = 0.13$	$\mu = 0.94$ $\sigma = 0.15$

homogenization in case of 2D simulations (see Table 4). These results correspond to those of the earlier study (Ref 26), in which merely 2D simulations were conducted.

Moreover, by comparing the results of the 3D simulations (Table 3) with the ones from 2D simulations (Table 4), it is seen that the 3D simulations have led to higher values especially for Young's Moduli. Because the voids in 2D models are considered to be continuous through the third direction (z direction) and not constrained along this axis, it is an expected result that, the 3D models, in which the voids are discrete and distributed non-uniformly, are stiffer than the 2D models for both homogenization methods. Similarly, the thermal conductivity of the 3D model is higher than the 2D models because the heat flow along the third axis has more degrees of freedom in case of 3D models. Since thermally sprayed YSZ coatings in general consist of non-uniformly distributed voids which do not lie continuously along the whole length of one of the

in-plane directions, the numerical calculations conducted in 2D domain underestimate the effective properties of the thermally sprayed coatings. This effect also explains the importance of the definition of the value of h in 3D models (distance between the 2D images) for an accurate determination of the effective properties. Therefore, the variation in Young's moduli with respect to different spacing distances between 2D images has been analyzed further. In Fig. 5, it is seen that Young's moduli calculated using 3D simulations decrease and get closer to the mean results of the 2D simulations as the distance between 2D images (h) increases. Since the modeling of a 3D structure with a 2D model is based on the assumption that the 2D cross section of the structure repeats itself in the third direction infinitely, it is expected that the solutions of the 3D models, which are reconstructed using the same 2D cross sections like 2D models, converge to the mean results of the 2D models, as h tends to infinity.

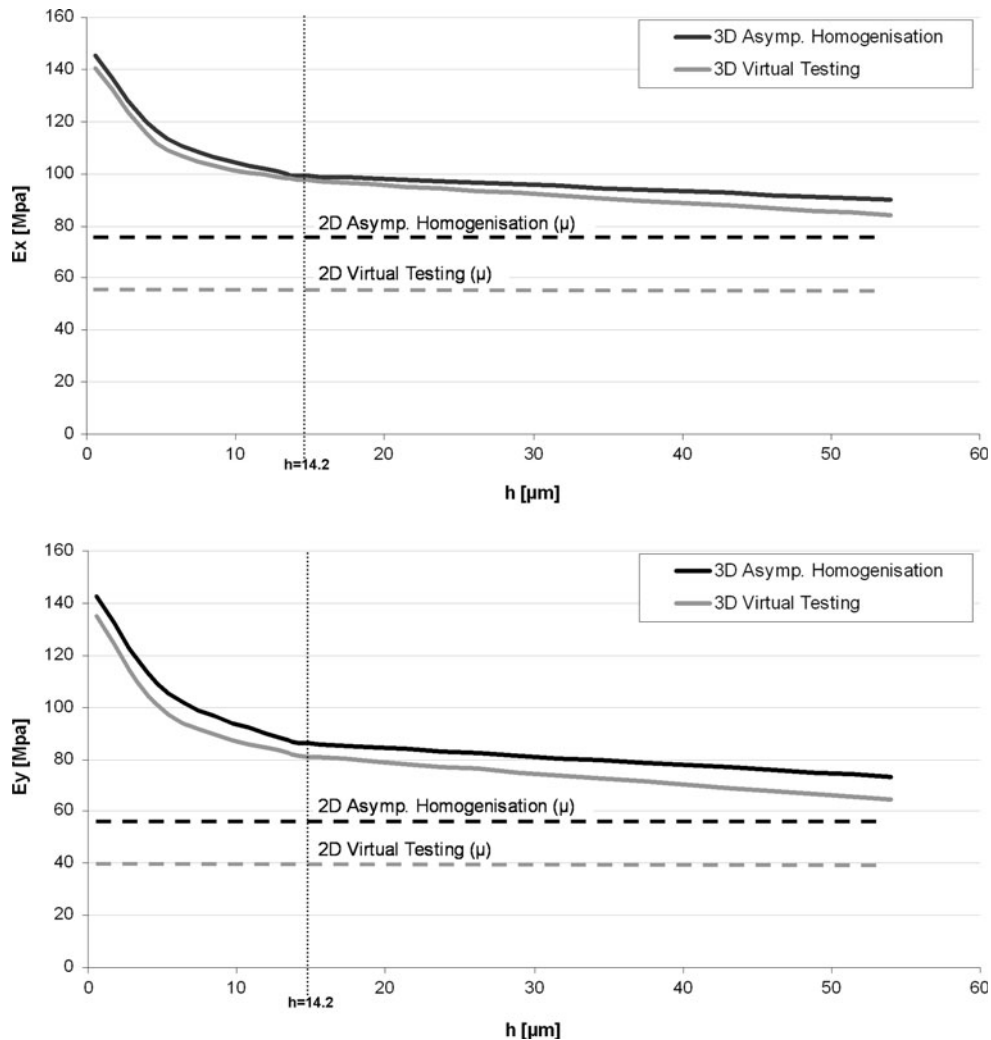


Fig. 5 Calculated values of effective Young's Moduli of the coating with respect to the value of the h

One should pay attention that the predictive capability of the models, which are based on the statistical 3D reconstruction approach, depends significantly on the definition of the distance between each pair of 2D images (h). 3D models with an oversized value of h would underestimate the effective properties. On the other hand, an undersized h value would lead to an overestimation of the effective properties.

6. Summary and Conclusion

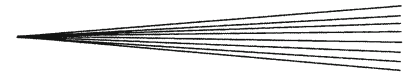
When using 3D models, the results of the virtual testing and asymptotic homogenization methods match each other more closely compared with the conventional 2D models. For the calculations conducted in 3D domain, both methods can be implemented interchangeably to estimate the effective properties without causing any significant difference. 2D models underestimate the effective properties of thermally sprayed YSZ coatings. The statistical 3D reconstruction approach developed in the context of this

study has been employed to calculate the effective properties of a typical YSZ coating in 3D domain. The calculated effective values of Young's Moduli and the thermal conductivity of the coating, which have been calculated by means of homogenization methods, agree with the results of microindentation and laser flash measurements. The definition of the distance between 2D images (h), which are used to reconstruct the 3D representation, is critical for the correctness of the calculated effective properties.

By means of a software tool, which will be developed by combining the codes and macros used in this study, the process steps of the presented methodology will be automated. Furthermore, the approach will be further developed to determine the effective properties of alloy coatings which involve characteristically more than two different distinguishable constituents.

Acknowledgments

The authors would like to thank the German Research Foundation DFG for the support of the depicted research



within the Cluster of Excellence “Integrative Production Technology for High-Wage Countries”.

References

1. F. Kroupa, Nonlinear Behaviour in Compression and Tension of Thermally Sprayed Ceramic Coatings, *J. Therm. Spray Technol.*, 2007, **16**(1), p 84-95
2. I.O. Golosnoy, A. Cipitria, and T.W. Clyne, Heat Transfer Through Plasma-Sprayed Thermal Barrier Coatings in Gas Turbines: A Review of Recent Work, *J. Therm. Spray Technol.*, 2009, **18**(5-6), p 809-821
3. I. Sevostianov and M. Kachanov, Elastic and Conductive Properties of Plasma-Sprayed Ceramic Coatings in Relation to Their Microstructure: An Overview, *J. Therm. Spray Technol.*, 2009, **18**(5-6), p 822-834
4. S. Deshpande, A. Kulkarni, S. Sampath, and H. Herman, Application of Image Analysis for Characterization of Porosity in Thermal Spray Coatings and Correlation with Small Angle Neutron Scattering, *Surf. Coat. Technol.*, 2004, **187**(1), p 6-16
5. T. Wiederkehr, B. Klusemann, D. Gies, H. Müller, and B. Svendsen, An Image Morphing Method for 3D Reconstruction and FE-Analysis of Pore Networks in Thermal Spray Coatings, *Comput. Mater. Sci.*, 2010, **47**(4), p 881-889
6. O. Amsellem, K. Madi, F. Borit, D. Jeulin, V. Guipont, M. Jeandin, E. Boller, and F. Pauchet, Two-Dimensional (2D) and Three-Dimensional (3D) Analyses of Plasma-Sprayed Alumina Microstructures for Finite-Element Simulation of Young's modulus, *J. Mater. Sci.*, 2008, **43**(12), p 4091-4098
7. O. Amsellem, F. Borit, D. Jeulin, V. Guipont, M. Jeandin, E. Boller, and F. Pauchet, Three-Dimensional Simulation of Porosity in Plasma-Sprayed Alumina Using Microtomography and Electrochemical Impedance Spectrometry for Finite Element Modeling of Properties, *J. Therm. Spray Technol.*, 2011, **21**(2), p 193-201
8. E. Lugscheider, R. Nickel, S. Kundas, and T. Kashko, A Homogeneous Material Model Approach of an APS-Sprayed PYSZ-TBC Considering the APS-Process-Parameters and the TBC-Microstructure, *Thermal Spray 2004: Advances in Technology and Application*, Vol 1129, May 10-12, 2004 (Osaka, Japan), ASM International, 2004, p 311-316
9. A.D. Jadhav, N.P. Pature, E.H. Jordan, M. Gell, P. Miranzo, and E.R. Fuller, Jr., Low-Thermal-Conductivity Plasma-Sprayed Thermal Barrier Coatings with Engineered Microstructures, *Acta Mater.*, 2006, **54**(12), p 3343-3349
10. Y. Tan, J.P. Longtin, and S. Sampath, Modeling Thermal Conductivity of Thermal Spray Coatings: Comparing Predictions to Experiments, *J. Therm. Spray Technol.*, 2006, **15**(4), p 545-552
11. V. Cannillo, L. Lusvardi, C. Siligardi, and A. Sola, Prediction of the Elastic Properties Profile in Glass-Alumina Functionally Graded Materials, *J. Eur. Ceram. Soc.*, 2007, **27**, p 2393-2400
12. F. Azarmi, T. Coyle, and J. Montaghimi, Young's Modulus Measurement and Study of the Relationship Between Mechanical Properties and Microstructure of Air Plasma Sprayed Alloy 625, *Surf. Coat. Technol.*, 2009, **203**, p 1045-1054
13. A. Zivelonghia, A. Brendela, S. Lindiga, S. Nawkab, B. Kieback, and J.H. You, Microstructure-Based Analysis of Thermal and Mechanical Behaviors of W/CuCrZr Composites and Porous W Coating, *J. Nucl. Mater.*, 2011, **417**(1-3), p 536-539
14. B. Klusemann, R. Denzer, and B. Svendsen, Microstructure-Based Modeling of Residual Stresses in WC-12Co-Sprayed Coatings, *J. Therm. Spray Technol.*, 2011, **21**(1), p 96-107
15. R. Bolot, J.L. Seicheoine, J.H. Qiao, and C. Coddet, Predicting the Thermal Conductivity of AlSi/Polyester Abradable Coatings: Effects of the Numerical Method, *J. Therm. Spray Technol.*, 2011, **20**(1-2), p 39-47
16. W. Tillmann, B. Klusemann, J. Nebel, and B. Svendsen, Analysis of the Mechanical Properties of an Arc Sprayed WC-FeCSiMc Coating: Nanoindentation and Simulation, *J. Therm. Spray Technol.*, 2011, **20**(1-2), p 328-335
17. R. McPherson, A Model for the Thermal Conductivity of Plasma-Sprayed Ceramic Coatings, *Thin Solid Films*, 1984, **112**(1), p 89-95
18. P.G. Klemens, Thermal Conductivity of Inhomogeneous Media, *High Temp. High Press.*, 1991, **23**, p 241-248
19. T.J. Lu, C.G. Levi, H.N.G. Wadley, and A.G. Evans, Distributed Porosity as a Control Parameter for Oxide Thermal Barriers Made by Physical Vapor Deposition, *J. Am. Ceram. Soc.*, 2001, **84**(12), p 2937-2946
20. C.-J. Li and A. Ohmori, Relationships Between the Microstructure and Properties of Thermally Sprayed Deposits, *J. Therm. Spray Technol.*, 2002, **11**(3), p 365-374
21. I.O. Golosnoy, S.A. Tripas, and T.W. Clyne, An Analytical Model for Simulation of Heat Flow in Plasma-Sprayed Thermal Barrier Coatings, *J. Therm. Spray Technol.*, 2005, **14**(2), p 205-214
22. R. Hill, Elastic Properties of Reinforced Solids: Some Theoretical Principles, *J. Mech. Phys. Solids*, 1963, **11**, p 357-372
23. D. Trias, J. Costa, A. Turon, and J.E. Hurtado, Determination of the Critical Size of a Statistical Representative Volume Element (SRVE) for Carbon Reinforced Polymers, *Acta Mater.*, 2006, **54**, p 3471-3484
24. G. Laschet, T. Kashko, S. Benke, M. Öte, and K. Bobzin, Chapter 5: Prediction of Effective Properties, *Integrative Computational Materials Engineering*, G.J. Schmitz and U. Prah, Eds., April 18, 2012, Wiley-VCH, 2012, p 101
25. G. Laschet, Homogenization of the Thermal Properties of Transpiration Cooled Multi-Layer Plates, *Comput. Meth. Appl. Mech. Eng.*, 2002, **191**, p 4535-4554
26. K. Bobzin, N. Bagcivan, D. Parkot, T. Kashko, G. Laschet, and J. Scheele, Influence of the Definition of the Representative Volume Element on the Effective Thermoelastic Properties of Thermal Barrier Coatings with Random Microstructure, *J. Therm. Spray Technol.*, 2009, **18**(5-6), p 988-995
27. S.A. Langer, E.R. Fuller, and W.C. Carter, Oof: An Image-Based Finite-Element Analysis of Material Microstructures, *Comput. Sci. Eng.*, 2011, **3**(3), p 15-23
28. A.C. Reid, S.A. Langer, R.C. Lua, V.R. Coffman, S. Haan, and R.E. Garca, Image-Based Finite Element Mesh Construction for Material Microstructures, *Comput. Mater. Sci.*, 2008, **43**(4), p 989-999
29. R. Nickel, “Die beschichtungsprozessabhängige Materialmodellierung von EB-PVD und APS-Wärmedämmschichten,” Ph.D. Thesis, Surface Engineering Institute of RWTH Aachen University, 2007, p 47-55 (in German)
30. Metallic materials—Instrumented Indentation Test for Hardness and Materials Parameters, ISO 14577-1:2002, Part 1: Test Method, 2002, p 17
31. H. Kaßner, “Theoretische und experimentelle Untersuchungen zum Plasmaspritzen mit nanoskaligen Suspensionen,” Ph.D. Thesis, Ruhr University Bochum, 2009, p 60 (in German)
32. H.J. Kim and Y.G. Kweon, Elastic Modulus of Plasma-Sprayed Coatings Determined by Indentation and Bend Tests, *Thin Solid Films*, 1999, **342**(1-2), p 201-206